RESEARCH ARTICLE

Removal of pharmaceutical compounds from aqueous solution by novel activated carbon synthesized from lovegrass (*Poaceae*)

Nilton F.G.M. Cimirro[1] · Eder C. Lima[2] · Mariene R. Cunha[1] · Silvio L. P. Dias[2] · Pascal Silas Thue[2] · Ana C. Mazzocato[3] · Guilherme L. Dotto[4] · Marcos A. Gelesky[5] · Flávio André Pavan[1]

Abstract

In this work, lovegrass (*Cpa*), an abundant grass of the *Poaceae* family, was employed as feedstock for the production of activated carbon in a conventional furnace using $ZnCl_2$ as a chemical activator. The prepared material (*Cpa*-AC) was characterized by pH of the point of zero charges (pH_{pzc}), Boehm's titration method, CHN/O elemental analysis, ATR-FTIR, N_2 adsorption/desorption curves, and SEM. This carbon material was used for adsorption of acetylsalicylic acid (ASA) and sodium diclofenac (DFC). FTIR analysis identified the presence of O-H, N-H, O-C=O), C-O, and aromatic ring bulk and surface of (*Cpa*-AC) adsorbent. The quantification of the surface functional groups showed the presence of a large amount of acidic functional groups on the surface of the carbon material. The isotherms of adsorption and desorption of N_2 confirm that the *Cpa*-AC adsorbent is mesopore material with a large surface area of $1040 \ m^2 \ g^{-1}$. SEM results showed that the surface of *Cpa*-AC is rugous. The kinetic study indicates that the system followed the pseudo-second-order model (pH 4.0). The equilibrium time was achieved at 45 (ASA) and 60 min (DCF). The Liu isotherm model best fitted the experimental data. The maxima sorption capacities (Q_{max}) for ASA and DFC at 25 °C were $221.7 \ mg \ g^{-1}$ and $312.4 \ mg \ g^{-1}$, respectively. The primary mechanism of ASA and DFC adsorption was justified considering electrostatic interactions and π-π interactions between the *Cpa*-AC and the adsorbate from the solution.

Keywords Lovegrass · Conventional pyrolysis · Activated carbon · Pharmaceuticals contaminants · Adsorption

✉ Flávio André Pavan
flaviopavan@unipampa.edu.br

Nilton F.G.M. Cimirro
niltonfmgelos@gmail.com

Eder C. Lima
profederlima@gmail.com

Mariene R. Cunha
mariene.cunha15@gmail.com

Silvio L. P. Dias
silvio@iq.ufrgs.br

Pascal Silas Thue
pascalsilasthue@gmail.com

Ana C. Mazzocato
acmazzocato@gmail.com

Guilherme L. Dotto
guilherme_dotto@yahoo.com.br

[1] Postgraduate Program in Engineering, Federal University of Pampa (UNIPAMPA), Bagé, RS 96412-420, Brazil

[2] Federal University of Rio Grande do Sul (UFRGS), Porto Alegre, RS, Brazil

[3] Brazilian Agricultural Research Corporation (EMBRAPA-CPPSul), Bagé, RS, Brazil

[4] Chemical Engineering Department, Federal University of Santa Maria (UFSM), Santa Maria, RS, Brazil

[5] School of Chemistry and Food, Federal University of Rio Grande (FURG), Rio Grande, RS, Brazil

Introduction

Pharmaceutical compounds play an essential role in preventing and treating human and animal diseases (Huerta-Fontela et al. 2011; Sotelo et al. 2012). Growing population and the search for a cure for new and old diseases have significantly increased the use of pharmaceuticals worldwide (Sotelo et al. 2014). The excessive increase in drug use occurs, an increase in the disposal of these compounds in the environment. These chemical compounds can be released into the environment in a variety of ways (Kummerer 2001; Marques et al. 2017). After administration, a significant part of the original pharmaceuticals and its metabolites is excreted through human and animal urine and feces, reaching in domestic sewage, industrial and hospital effluents, soil, and aquatics ecosystems (Bolong et al. 2009; Taylor and Senac 2014; Pouretedal and Sadegh 2014). The inappropriate disposal of disused and overpowered pharmaceuticals has contributed to the increase in the incidence of it in the environment (European community 2015, Suriyanon et al. 2013).

After dispersed to the environment, these chemical compounds can compromise water and soil quality by compromising human and animal health (European community 2015; Secondes et al. 2014).

The presence of pharmaceuticals on domestic and industrial wastewaters was detected in the waters of different countries (European community 2015; Zuccato et al. 2010; Elmolla and Chaudhuri 2010; Ginebreda et al. 2010; Fatta-Kassinos et al. 2011). Pharmaceuticals are very persistent and poorly biodegradable compounds and may be hazardous in aquatic life even at low concentrations (Homem et al. 2013). For this reason, environmental regulatory agencies around the world have given additional attention in monitoring these chemical compounds in waters (Sotelo et al. 2012; European community 2015).

There are several treatment methods available that can be employed for the removal of pharmaceutical compounds from aqueous media (Chun et al. 2015; Homayoonfal and Mehrnia 2014; Sophia and Lima 2018; Deegan et al. 2011). The adsorption technique using powdered activated carbon as adsorbent has been considered adequate for the removal of various organic contaminants from water, including pharmaceuticals (Chayid and Ahmed 2015). The extensive utilization of granular-activated carbon in the adsorption process is due to its characteristics such as high surface area, good pore structure, and medium regeneration capacity (Moussavi et al. 2013).

The use of botanical biomasses as a feedstock material for the manufacture of low-cost-activated carbons with specific properties has gained interest in the scientific community (Wong et al. 2018a, b). Studies show that activated coals produced from agricultural biomass are quite competitive when compared with commercial-activated carbon due to low-cost,

elevated sorption capacity, and reuse possibility (Kasperiski et al. 2018b; Lima et al. 2019). There are many examples of the use of botanical biomasses employed for the manufacture of activated carbon as an adsorbent for water and wastewater treatments (Sophia and Lima 2018; Liu et al. 2017; Leite et al. 2018).

Tsai et al. (2020) proposed the use of cocoa pod husk as a carbon precursor, and it was chemically activated using KOH using different temperatures (400–800 °C) obtaining activated carbons with BET surface area (S_{BET}) ranging from 6 to 1783 $m^2 g^{-1}$. Briton et al. (2020) developed activated carbons from plantain (*Musa* × p*aradisiaca)* spike waste using response surface methodology. This biomass was chemically activated using H_3PO_4 as an activating specie. Bhomick et al. (2020) studied the biomass of *Schima wallichii* that was doubly pyrolyzed in a conventional furnace. First, it was pyrolyzed at 600 °C under nitrogen flow. Afterward, it was impregnated with $ZnCl_2$ and finally pyrolyzed at 500–700 °C. The activated carbons obtained presented S_{BET} ranging from 269 to 999 $m^2 g^{-1}$. Lima et al. (2019) prepared activated carbon from capsules of cashew of Para using chemical activation with $ZnCl_2$. The biomass was pyrolyzed at 600–700 °C, obtaining S_{BET} ranging from 1419 to 1457 $m^2 g^{-1}$. Based on these works, it is possible to infer that different biomasses using different conditions of pyrolysis and chemical activators can obtain different activated carbons with different surfaces to adsorb different species of interest (Sophia and Lima 2018).

In the context of developing new activated carbons, up to our best knowledge, works reporting the use of lovegrass grass as a carbon feedstock to produce activated carbon by convention pyrolysis, and its application for acetylsalicylic acid and diclofenac has not been found in the literature.

Lovegrass known botanically as *Eragrostis plana* Nees belonging to the family of *Poeacea* is an abundant non-toxic and renewable ecological material very commonly found in all Brazilian regions (Filho et al. 2017). This vegetable biomass contains in its composition considerable amounts of cellulose, hemicellulose, and lignin that make this plant interesting precursor material for the manufacture of activated carbon (Wong et al. 2018a, b; Gonzáles-Garcia 2018).

The lovegrass is an invasive species on the farms of Brazil (Barbosa et al. 2013). It presents a low nutritional value and high mechanical traction strength. Therefore it is not appropriate for cattle breeding. Therefore, the lovegrass is unsuitable for grazing (Scheffer-Basso et al. 2016). Its presence on the Brazillian farms brings economic losses for farmers. (Barbosa et al. 2013). This work aims to add valor to lovegrass.

In this context, this study aims to produce activated carbon from lovegrass by conventional pyrolysis using chemical activation and its application as an adsorbent for removal two pharmaceutical compounds, acetylsalicylic acid (analgesic),

and diclofenac sodium (anti-inflammatory) both widely used by the world population and frequently detected in aquatic ecosystems. The produced activated carbon produced from lovegrass was characterized by pH of the point of zero charges (pH$_{pzc}$), Boehm's titration method, CHN/O elemental analysis, FTIR, N$_2$ adsorption/desorption curves, and SEM. The adsorption studies were performed by the batch process, considering the adsorption capacity. Kinetic and equilibrium studies were also performed, and the effects of pH, contact time, initial concentration, and adsorbent mass were investigated to understand the mechanism of interaction between adsorbate-adsorbent.

Material and methods

Chemicals and biomass source

The acetylsalicylic acid (ASA) and sodium diclofenac (DFC) (see Supplem. Fig. S1 and Fig. S2, respectively) chemical were obtained from Merck and were of analytical grade. The ultrapure water was used to prepare all working solutions.

Ten kilograms of lovegrass leaves were collected on a farm of the University of Federal Pampa, Bagé town, in the State of Rio Grande do Sul, Brazil. The lovegrass leaves were washed abundantly with tap water and dried at 60 °C for 3 days. Afterward, it was milled and sifted to obtain particle size ≤ 250 μm, which will facilitate the reaction during activation. Analytical grade zinc chloride (ZnCl$_2$) was used as an activating agent (Synth, Diadema, Brazil).

Preparation of Cpa-AC-activated carbon

The Cpa-AC material was prepared by chemical activation at an impregnation ratio of 1:1 (biomass precursor:ZnCl$_2$), followed by pyrolysis in a conventional furnace. The activated carbon adsorbent was prepared as follows: dried biomass precursor (particle size between 50 and 60 μm) was impregnated in solution with the chemical activating at 80 °C for 120 min. After, the mixture was pyrolyzed at 700 °C in a horizontal furnace, using a ramp heating of 10 °C/min under N$_2$ flow (200 mL/min) for 1 h. The activated material was cooled and treated with 6 mol/L HCl under reflux at 80 °C, filtered, and washed deionized water several times until the pH neutral (Puchana-Rosero et al. 2016; Umpierres et al. 2018). Then, it was dried in an oven at 100 °C for 24 h. Afterward, the carbon adsorbent was ground and sieved, and it was called as Cpa-AC.

Characterization of Cpa-AC adsorbent

Elemental composition CHN of biomass (Cpa) and activated carbon (Cpa-AC) were obtained by the Elemental Analyzer (Perkin Elmer, Waltham, MA, USA). The difference between total percentage (100wt%) and the sum of percentages (W% dry ash-free) of nitrogen, hydrogen, and carbon was used to obtain the oxygen content (Thue et al. 2016).

The surface composition of biomass precursor (Cpa) and the produced activated carbon (Cpa-AC) were characterized using spectrophotometer model FTIR-8400S (Shimadzu, Japan), combined with the ATR accessory.

The total surface basicity and acidity of Cpa-AC material were quantified by the modified method of Boehm titration (Oickle et al. 2010).

The pore size and surface area of Cpa-AC were calculated by the BJH and BET methods using N$_2$ at − 196 °C utilizing an adsorption analyzer (Micromeritics Instrument, TriStar II 3020) (Pavan et al. 2002; Wamba et al. 2019).

The point of zero charges (pH$_{pzc}$) of Cpa-AC was obtained as previously described in our study (Umpierres et al. 2018).

Scanning electron microscopy technique (SEM) using a JEOL Electron Microscope operating at 15 kV was employed to verify the morphology biomass precursor (Cpa) and Cpa-AC carbon.

ASA and DFC adsorption onto Cpa-AC

The adsorption studies of ASA and DFC on Cpa-AC adsorbent were performed using a typical batch procedure at 25 °C. The adsorption studies were carried out as follows: An amount of mass (30.0–200.0 mg) of Cpa-AC was added to solutions of pharmaceutical compounds at different initial concentrations and pH solution values (2.0–10.0). The mixtures were then shaken at 200 rpm and collected at the desired contact time (see details on kinetic assays). After centrifugation, the amounts of pharmaceuticals in the supernatant solution were determined UV spectrophotometry using a UV-Vis spectrophotometer (Agilent, Cary 50 Bio, Santa Clara, USA) at a maximum absorption wavelength of ASA (280 nm) and DFC (275 nm). Eqs. (1) and (2) respectively calculated the sorption capacity (q) of adsorbate adsorbed on Cpa-AC and the percentage of removal.

$$q = \frac{(\text{Co-Cf})}{m} x\text{V} \qquad (1)$$

$$\%\text{Removal} = 100x\frac{(\text{Co-Cf})}{\text{Co}} \qquad (2)$$

where q is the sorption capacity of Cpa-AC (mg g^{-1}), C_f is final ASA or DFC concentration after adsorption (mg L^{-1}), C_o is the initial ASA or DFC concentration in contact with Cpa-AC (mg L^{-1}), m is the mass of Cpa-AC (g), and V is the volume of ASA or DFC solution (L).

Kinetic models

Kinetic adsorption studies were made using 60 mg of *Cpa*-AC adsorbent for 20 ml of pharmaceutical solution (200.0 and 400.0 mg L^{-1}). The samples were withdrawn at different times varying between 5 and 120 min at pH solution value 4.0 pseudo-first-order, pseudo-second-order, and Avrami fractional-order (Lima et al. 2012) models were used to fit the kinetic data. The mathematical equations of these respective models are shown in Eqs. (3), (4), and (5).

$$q_t = q_e x[1\text{-exp}(\text{-k}_1 xt)] \tag{3}$$

$$q_t = \frac{q_e^2 k_2 t}{[k_2(q_e)xt + 1]} \tag{4}$$

$$q_t = q_e x\left\{1\text{-exp}[\text{-(k}_{AV}xt)]^{nAV}\right\} \tag{5}$$

where k_1 is the pseudo-first-order rate constant (min^{-1}), k_2 is the pseudo-second-order rate constant (g mg^{-1} min^{-1}), t is contact time (min), q_t and q_e are the amounts of adsorbate adsorbed at time t and the equilibrium (mg g^{-1}).

Equilibrium models

For the equilibrium studies, an amount of 60 mg of *Cpa*-AC was added to 20.0 mL solution of pharmaceutical compounds at the concentration ranging from 100.0 to 2000.0 mg L^{-1}, at pH 4.0 value. The mixture was stirred for 60 min, and the concentrations of ASA or DFC remaining in the solution were calculated.

Langmuir, Freundlich, and Liu's models were employed for analysis of equilibrium data. Equations 6, 7, and 8 show the corresponding Langmuir, Freundlich, and Liu models (Lima et al. 2012).

$$q_e = \frac{Q_{max} x K_L x C_e}{1 + K_L x C_e} \tag{6}$$

$$q_e = K_F x C_e^{1/n_F} \tag{7}$$

$$q_e = \frac{Q_{max} x \left(K_g x C_e\right)^{n_L}}{1 + \left(K_g x C_e\right)^{n_L}} \tag{8}$$

where q_e is the adsorbate amount adsorbed at equilibrium (mg g^{-1}); C_e is the adsorbate concentration at equilibrium (mg L^{-1}); Q_{max} is the maximum sorption capacity of the adsorbent (mg g^{-1}); K_L is the Langmuir equilibrium constant (L mg^{-1}); K_F is the Freundlich equilibrium constant (mg g^{-1}.(mg L^{-1})$^{-1/nF}$); K_g is the Liu equilibrium constant (L mg^{-1}); n_F and n_L are the exponents of Freundlich and Liu model, respectively, (n_F and n_L are dimensionless).

Statistical evaluation of models and quality control

The preliminary experiments were carried out to ensure reproducibility, reliability, and accuracy of the experimental data. The relative standard deviations of all measurements were below 5% (Lima et al. 1999, b). Blanks were run in parallel and corrected when necessary (Lima et al. 2000).

The solutions of ASA and DFC were stored in glass bottles, which were cleaned, rinsed with deionized water, dried, and stored them in a suitable cabinet (Lima et al. 2003).

Standard ASA and DFC solutions (2.0–80.0 mg L^{-1}) were used for calibration in parallel with a blank. The linear analytical calibration curve was performed on the UV-VIS software of the Agilent, Cary 50 Bio spectrophotometer. All the analytical measurements were carried out in triplicate, and the precisions of the standards were better than 3.4% ($n = 3$) (Lima et al. 1998b).

The detection limits of ASA and DFC were 0.20 and 0.18 mg L^{-1}, respectively, with a signal/noise ratio of 3 (Lima et al. 1998a).

The kinetic and equilibrium data fitness was carried out with nonlinear methods, which were evaluated using the Simplex method and the Levenberg–Marquardt algorithm using the fitting facilities of the Microcal Origin 2018 software [36, 37]. The adequacy of the equilibrium and kinetic models was evaluated using the determination coefficient (R^2), the adjusted determination coefficient (R^2_{adj}), and the standard deviation of residues (SD) (Lima et al. 2012; Kasperiski et al. 2018a, b; Pavan et al. 2008).

Mathematical expressions for respective R^2, R^2_{adj}, and SD are presented in Eqs. (9), (10), and 11, respectively.

$$R^2 = \left(\frac{\sum_i^n \left(q_{i,exp}\text{-}\overline{q}_{exp}\right)^2 \text{-} \sum_i^n \left(q_{i,exp}\text{-}q_{i,model}\right)^2}{\sum_i^n \left(q_{i,exp}\text{-}\overline{q}_{exp}\right)^2}\right) \tag{9}$$

$$R^2_{adj} = 1\text{-}\left(1\text{-}R^2\right)x\left(\frac{n\text{-}1}{n\text{-}p\text{-}1}\right) \tag{10}$$

$$SD = \sqrt{\left(\frac{1}{n\text{-}p}\right)x\sum_i^n (qi, exp\text{-}qi, model)2} \tag{11}$$

where $q_{i,exp}$ is particular experimental q value; $\overline{q}_{exp}$ is the average of all experimental q values measured; $q_{i,model}$ is individual theoretical q value predicted by the model; p is the number of parameters in the fitting model, and n is the number of experiments.

Results and discussions

Characterization of the *Cpa*-AC adsorbent

The elemental composition CHN/O of *Cpa* and *Cpa*-AC material was obtained. The results show that *Cpa* presented

48.25% C, 6.10% H, 2.35% N, and 39.64% O. When the sample was pyrolyzed, the C content increases to 71.77%, while the H, N, and O percentages drastically diminished to 2.59%, 2.33%, and 17.50%, respectively. The increase in the amount of carbon after the pyrolysis process can be explained due to the predominant aromatic structure of the *Cpa*-AC material whereas losses of H, N, and O are due to the thermal degradation of lignin, hemicellulose, and cellulose present in the *Cpa* biomass during the pyrolysis (Leite et al. 2018; Cunha et al. 2018).

The number of chemical groups present on the *Cpa*-AC adsorbent was quantified by the modified method of Boehm titration (Oickle et al. 2010). The total basicity and acidity were quantified with HCl and NaOH solutions, respectively (Umpierres et al. 2018; Cunha et al. 2018). The total basicity of *Cpa*-AC was 0.05 mmol g^{-1}, and the total acidity of *Cpa*-AC adsorbent was 1.540 mmol g^{-1}. These results confirm the acidic behavior of the surface of *Cpa*-AC adsorbent.

In this study, the FITR analysis was performed for to confirm the conversion of biomass precursor (*Cpa*) to derived activated carbon (*Cpa*-AC) and thus for to determine the chemical groups on (*Cpa*-AC) after the pyrolysis and chemical activation processes that may help on the ASA and DFC adsorption. Based on Fig. 1, if we compare the absorption spectra of the *Cpa* and the *Cpa*-AC, it is possible to verify that a difference exists between them. Fig. 1 shows that the absorption spectrum of *Cpa*-AC presents fewer and less intense absorption bands when compared with the spectrum of *Cpa*. The elimination of the chemical groups and created

aromatic ring verified in the *Cpa*-AC spectrum is indicative of the conversion satisfactory of the biomass precursor to activated carbon.

For the *Cpa* biomass, the strong band at 3323 cm^{-1} is attributed to O-H and N-H groups (Kasperiski et al. 2018a; Cunha et al. 2018). The two bands at 2850 and 2918 cm^{-1} were assigned to symmetric and asymmetric stretching of the C–H group, respectively (Umpierres et al. 2018). These two bands disappeared in the Cpa-AC carbon material. The band at 1732 and 1367 cm^{-1} was assigned to the O=C stretching of carboxylic groups (Umpierres et al. 2018; Thue et al. 2016). The small bands at 1423 and 1369 cm^{-1} are assigned to ring modes of the benzene ring (Umpierres et al. 2018; Kasperiski et al. 2018a, b). The small band at 1242 cm^{-1} could be assigned to the C-N stretch (Pavan et al. 2008; Cunha et al. 2018). The peaks at 1160 cm^{-1} correspond to the C-O stretch of secondary alcohols or ethers (Kasperiski et al. 2018a; Pavan et al. 2008); the band at 1030 cm^{-1} corresponds to the C-O stretch of primary alcohols (Kasperiski et al. 2018b; Yacob et al. 2015). The bands at 900 cm^{-1} are assigned to the bending of out-of-plane of H-C groups (Kasperiski et al. 2018a; Pavan et al. 2008).

In the characteristic spectrum of the *Cpa*-AC, it is possible to identify some adsorption bands corresponding to chemical groups such as alcohols and phenols, esters and carboxylic acids, and mainly aromatics remaining after the pyrolysis process. The absorption peak at 3354 cm^{-1} was attributed to the O-H and N-H vibrations (Filho et al. 2017; Cunha et al. 2018; Yacob et al. 2015). The band at and 1563 cm^{-1} is assigned to

Fig. 1 FTIR spectra of the *Cpa* and *Cpa*-AC adsorbent
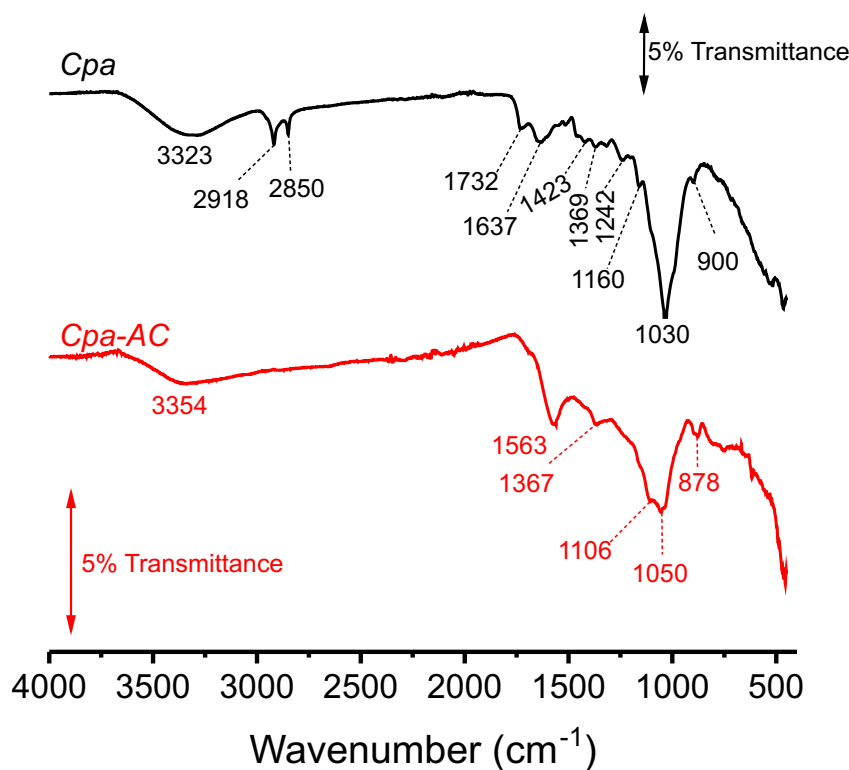
an asymmetric stretch of carboxylate (O-C=O) (Filho et al. 2017; Cunha et al. 2018; Yacob et al. 2015); the shoulder at 1367 cm^{-1} is due to the aromatic ring modes (Umpierres et al. 2018; Thue et al. 2016). The bands at 1106 cm^{-1} correspond to the C-O stretch of secondary alcohols (Umpierres et al. 2018; Kasperiski et al. 2018a); the band at 1050 cm^{-1} corresponds to the C-O stretch of primary alcohols (Pavan et al. 2008; Yacob et al. 2015). The bands at 808 cm^{-1} correspond to C-H out-of-plane bends of aromatic rings (Pavan et al. 2008; Yacob et al. 2015). FTIR analysis confirms the functional groups measured by the Boehm's titration method.

Pore size distribution is a factor essential for the better comprehension of the kinetic and equilibrium adsorption mechanism between adsorbent and adsorbate with distinct dimensions. The average pore diameter distribution of Cpa-AC, as well as the isotherm of adsorption and desorption of nitrogen, is presented in Fig. 2 a and b, respectively. Figure 2a shows that Cpa-AC adsorbent presents a pore size distribution between 2.8 and 50.6 nm of pore diameter. Fig. 2b reveals that the isotherm of adsorption and desorption of N$_2$ presents a

hysteresis of type IV, typical of the mesoporous materials (Pavan et al. 2002).

The specific surface area (S$_{BET}$) of Cpa-AC adsorbent was 1040 m^2 g^{-1}. From this value, the micropore area is 304.56 m^2 g^{-1}, and the external surface area of Cpa-AC adsorbent is 732.55 m^2 g^{-1}, which corresponds to 29.28% (micropore area) and 70.43% (external pore area) of the total S$_{BET}$. Moreover, Cpa-AC material exhibits a mesopore volume of 0.4675 cm^3 g^{-1} and a micropore volume of 0.1354 cm^3 g^{-1}. The percentages of the mesopore and micropore volume concerning the total pore volume are 77.52% and 22.45%, respectively (Cunha et al. 2018). Analyzing the results, it is possible to conclude that 77.52% of pore volume and 70.43% of the surface area are due to mesopores present on the structure of the novel Cpa-AC material.

SEM was used to study the morphology of the biomass before (Cpa) the carbonization and the Cpa-AC activated carbon after the carbonization. The electronic photomicrography of the Cpa and Cpa-AC materials are shown in Fig. 3 a and b, respectively. When analyzing the photos shown in Fig. 3 a and b, it is clear that there were significant differences morphological in the two materials. SEM photo of Cpa biomass (Fig. 3a)
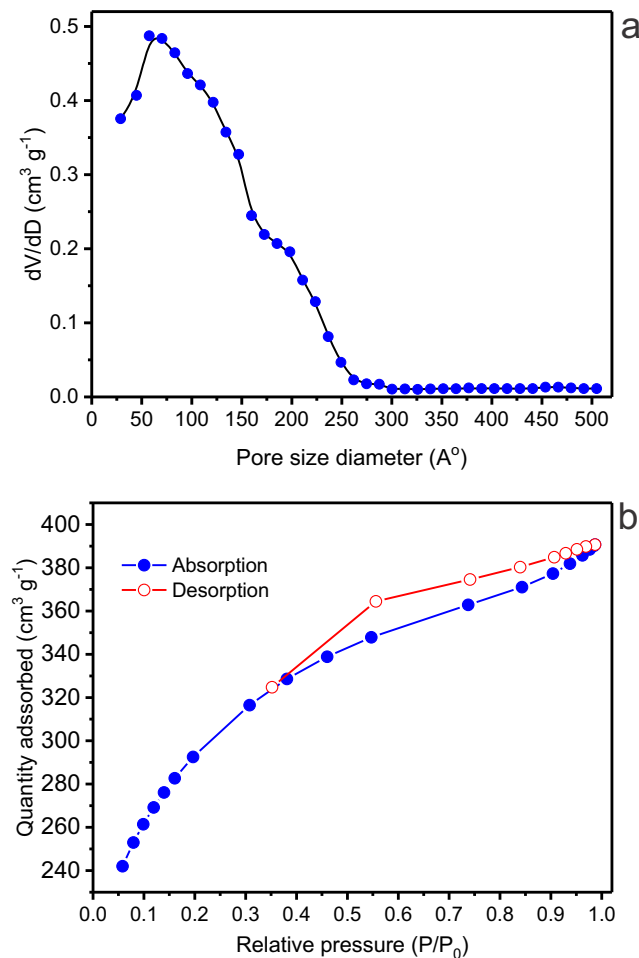

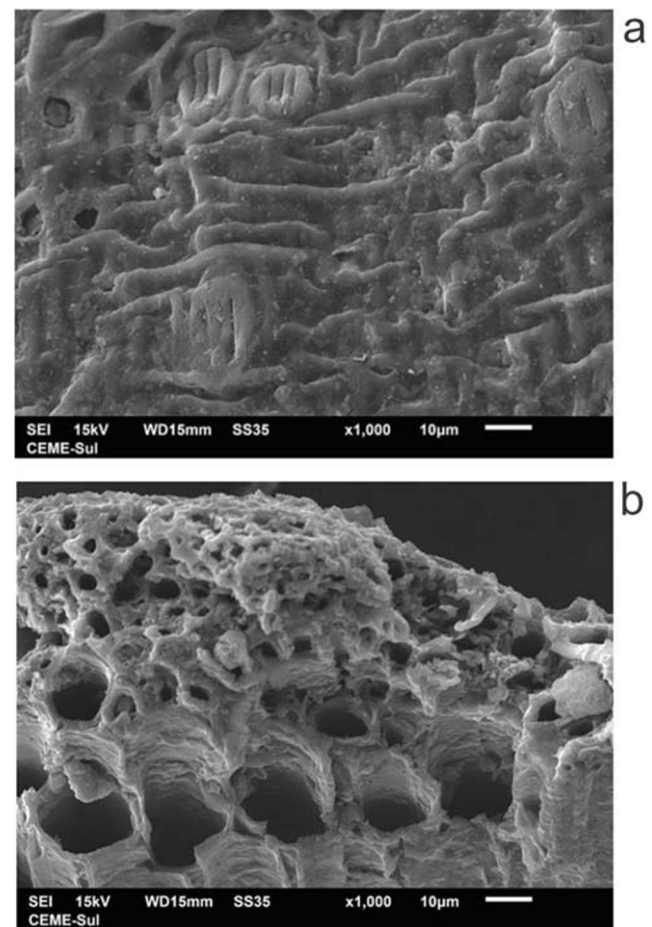Fig. 2 N$_2$ adsorption-desorption isotherm (a) BJH and (b) BET of Cpa-AC adsorbent

Fig. 3 SEM fotomicrographs (a) Cpa precursor and (b) Cpa-AC adsorbent

shows fiber and homogenous surface without cavities of the biomass. The SEM image of the *Cpa*-AC surface (Fig. 3b) reveals the presence of irregular pores and cavities over the surface of the material. These cavities and pores formed can be attributed to the chemical activation with $ZnCl_2$ (Lima et al. 2019; Wang et al. 2009). The SEM results confirm the stage of the carbonization with $ZnCl_2$ activation of the *Cpa* (Lima et al. 2019; Wang et al. 2009).

The point of zero charges (pH_{pzc}) is defined as the pH of the solution that lets the net charge of the solid surface as zero. This happens when the summation of all negative and positive charges on the solid surface is equivalent (Umpierres et al. 2018). The *Cpa*-AC surface will be positively charged when the pH of solutions is lower than pH_{pzc} (Cunha et al. 2018), and it will be negatively charged for the pH of solutions higher than pH_{pzc}. Figure 4 provides the plot of ΔpH versus initial pH values. The obtained value of pH_{pzc} for *Cpa*-AC adsorbent was 4.96. These results show the acidic behavior of the *Cpa*-AC surface, which is in agreement with the total acidity groups obtained by the Boehm titration method (the "Characterization of the *Cpa*-AC adsorbent" section).

Optimization of batch contact adsorption conditions

The adsorption experiments were carried out with ASA and DFC molecules in aqueous media. Different adsorbent masses (10–120 mg) of *Cpa*-AC material were mixed with 20.0 mL of the two pharmaceuticals solutions (10.0 to 1000.0 mg L^{-1}) with an initial pH of adsorbate solutions ranging from 2.0 to 10.0.

The effect of the initial pH of ASA and DFC solutions on adsorption capacity onto *Cpa*-AC adsorbent was evaluated (see Fig. 5). These results show that the values of adsorption capacities (q_e) of *Cpa*-AC adsorbent of practically do not change from pH values between 2.0 and around 4.5 for both
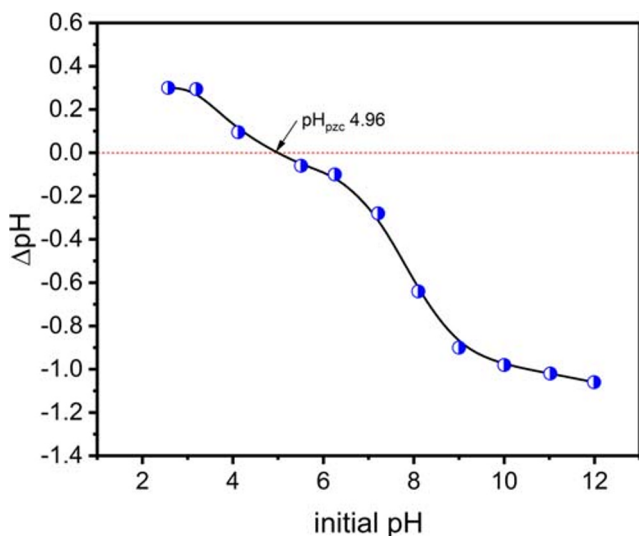
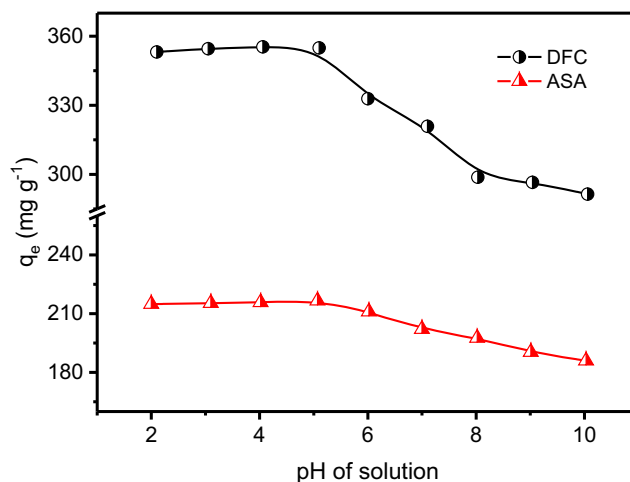**Fig. 5** Effect of pH of the pharmaceuticals adsorption onto *Cpa*-AC (**a**) ASA and (**b**) DFC. Conditions: $C_0 = 2000.0$ mg L^{-1}; T = 25 °C; adsorbent mass = 60.0 mg, and t = 60 min. The final pH of all the solutions was measured, and considering the acidic behavior of *Cpa*-AC, the final pH of the solutions decreases by 0.5 to 2.0 concerning the initial pH
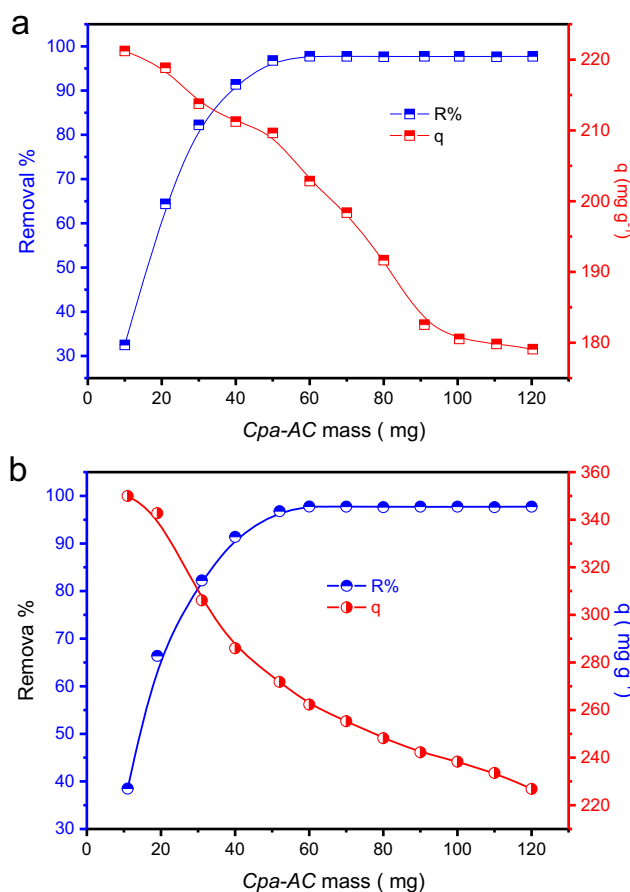
Fig. 6 Effect of the mass of the *Cpa*-AC on the adsorption. **a** ASA. **b** DFC. $C_0 = 2000.0$ mg L^{-1}; T = 25 °C; t = 60 min; and initial pH = 4.0. The final pH of the solutions was 3.5–3.8

Fig. 4 pHPCZ of *Cpa*-AC adsorbent

pharmaceutical compounds, while at pH values between 5.0 and 10.0, a decrease on adsorption capacities were observed. The behavior can be discussed considering the point of zero charges (pH$_{pzc}$) of *Cpa*-AC adsorbent, negative, and the positive charges of pharmaceutical compounds at pH values. Depending on the charges of both *Cpa*-AC adsorbent and ASA or DFC molecules, we will have an attraction or repulsion forces. The pH$_{pzc}$ of *Cpa*-AC adsorbent is acid (4.96) due to a large quantity of acidic functional groups present on the surface of the adsorbent. When pH < pH$_{pzc}$ value, the surface of *Cpa*-AC adsorbent is charged positively while ASA and DFC are charged negatively (pK$_a$ 3.41 and 4.00 for ASA and DCF, respectively) and contribute to the electrostatic attraction between then. Otherwise, for pH values between 5.0 and 10.0 (pHs > pH$_{pzc}$), a strong electrostatic repulsion between the negative surface of the adsorbent and the negative charges of ASA and DFC results in a decrease of adsorption capacities. However, other possibilities adsorption of ASA and DFC onto *Cpa*-AC adsorbent, such as $\pi - \pi$ interactions and hydrogen bonds, van der Waals forces should not be neglected (Filho et al. 2017; Kasperiski et al. 2018b; Cunha et al. 2018). Based on these results for the other adsorption studies of ASA and

DFC on *Cpa*-AC adsorbent, the pH of the solutions was adjusted to 4.0. The final pH of all the solutions was measured after the adsorption procedure. Considering that the *Cpa*-AC adsorbent presents an acidic behavior, all final pH of the solutions have a decrease of initial pH ranging from 0.5 to 2.0, when compared with the initial values of the adsorbate solutions.

The influence of the mass of *Cpa*-AC on ASA and DFC adsorption was performed with the increases of the quantity of adsorbent (10.0 to 120.0 mg) maintaining other parameters fixed as initial ASA and DFC initial pH 4.0, contact time (60.0 min), concentrations (400.0 mg L^{-1}), and shaker speed (150.0 rpm). The sorption capacity and the percentage of removal (%Rem) of ASA and DFC onto *Cpa*-AC adsorbent are shown in Fig. 6.

If we examine, Fig. 6a and b are possible to verify that when adsorbent mass was augmented from 10.0 to 60.0 mg, the %Rem of ASA rose from 32.50 to 97.80% (Fig. 6a) and the percentage of DCF removal increased from 41.60 to 98.08% (Fig. 6b). For adsorbent masses higher than 60.0 mg, the percentage of removal was practically constant (see Fig. 6). On the other hand, the sorption capacity (q) of
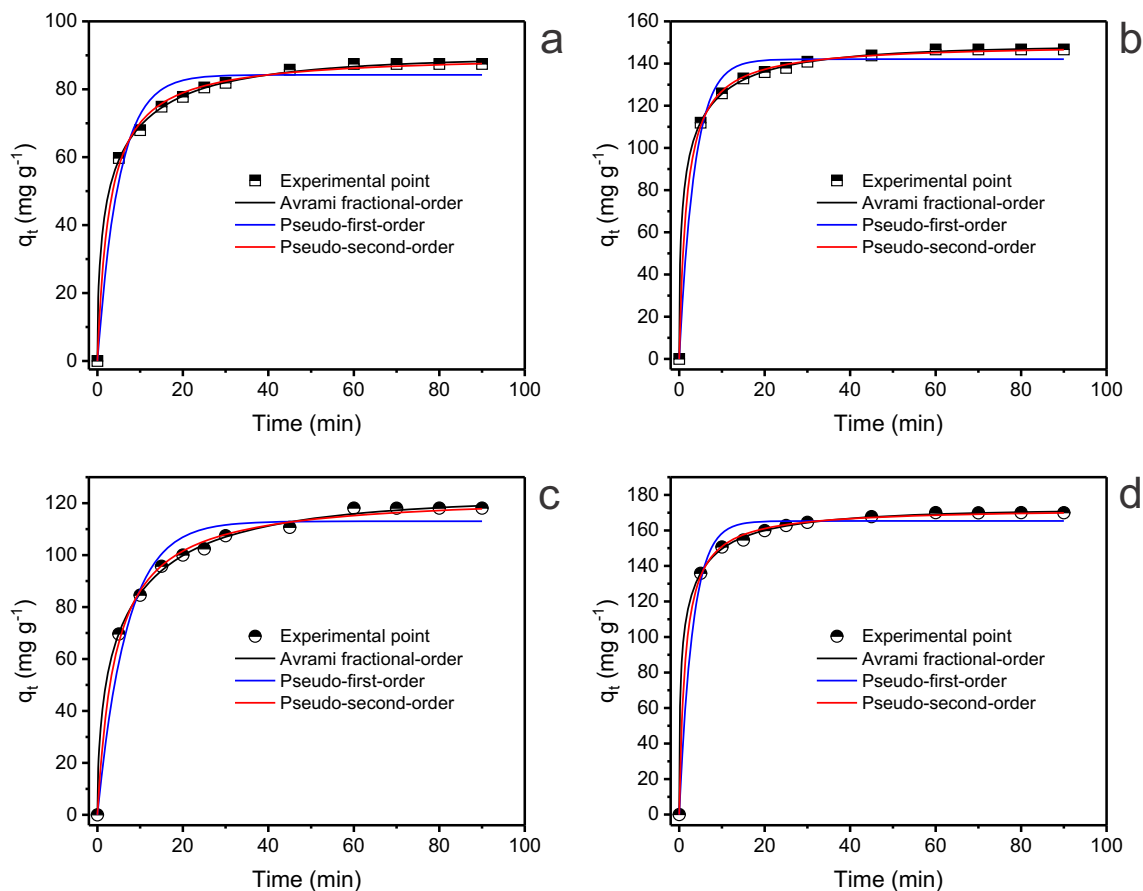

Fig. 7 Kinetic adsorption curves of (**a**) ASA 200.0 mg L^{-1}, (**b**) ASA 400.0 mg L^{-1}, (**c**) DFC 200.0 mg L^{-1}, and (**d**) DFC 400.0 mg L^{-1} using *Cpa*-AC adsorbent. Initial pH of adsorbate solution was fixed at

pH 4.0, temperature of 25 °C, and mass of adsorbent of 60 mg. The final pH of the solutions was within 3.5–3.8

both pharmaceuticals decreased for the increase of adsorbent mass from 10.0 to 120.0 mg. For this reason, 60 mg of Cpa-AC was chosen for the other experiments reported in this work. The sorption capacities were 202.84 mg g^{-1} for ASA and 252.36 mg g^{-1} for DCF, using 60 mg of Cpa-AC adsorbent.

Increases in %Rem of the ASA and DFC with masses of Cpa-AC material up to 60.0 mg could be attributed to an increase in the surface areas of the adsorbent available for sorbing the adsorbate (Pavan et al. 2008; Cunha et al. 2018). The most likely hypothesis for decreasing q with increased adsorbent mass is due to particulate aggregation of the solid adsorbent. Such aggregation of solid particles would cause a diminishing of the surface area of the adsorbent available for adsorption and augmentation in diffusional path length for the adsorbate to reach the active adsorbent sites (Pavan et al. 2008; Cunha et al. 2018).

Adsorption kinetics

The data of kinetics of adsorption of the ASA and DFC onto Cpa-AC adsorbent were assessed using the nonlinear kinetic models of the Avrami fractional-order, pseudo-first-order, and pseudo-second-order (Lima et al. 2012). The kinetic adsorption curves and the parameters of the kinetic model are depicted in Fig. 7 and Table 1.

The standard deviation (SD) and the adjusted determination coefficient (R^2_{adj}) were used to statistically evaluate the fitting of the kinetic data (Thue et al. 2016). The smaller discrepancy between the theoretical (calculated by the models) and experimental q values are obtained with lower SD and higher R^2_{adj} values (Thue et al. 2016). The kinetic parameters, SD, and R^2_{adj} are shown in Table 1. According to the results shown in Table 1, the best fitted kinetic model was the Avrami fractional-order. The Avrami fractional-order exhibited lower SD values (ranging from 0.5811 to 0.6818 (mg g^{-1}) for ASA and from 0.7464 to 1.352 for DFC) and highest R^2_{adj} values (0.9992–0.9998, for ASA and 0.9984–0.9998 for DFC, see Table 1). It was verified that the sorption capacity at any time (q_t) calculated by the Avrami fractional-order model is closest to the experimental values of q_t for both ASA and DFC pharmaceuticals.

Figure 7 shows the relationship between the sorption capacities at any time (q_t) of ASA and DFC (mg g^{-1}) with the contact time (min). The equilibrium time was 45 min for ASA (molecular volume 154.95 A^3) and 60 min for DFC (molecular volume 234.43 A^3). These results show that kinetic adsorption on Cpa-AC is relatively fast and that it depends on molecular volume. The smaller volume of the chemical molecule

Table 1 Kinetics parameters, R^2_{adj}, and SD for ASA and DFC adsorption onto Cpa-AC adsorbent. All numeric values are expressed with four significant digits

|	ASA		DFC	
Concentration (mg L^{-1})	200.0	400.0	200.0	400.0
Avrami fractional-order				
q_e (mg g^{-1})	89.78	148.8	122.4	172.2
k_{AV} (min^{-1})	0.2328	0.4555	0.1421	0.6382
n_{AV}	0.4602	0.4101	0.5025	0.3825
$t_{1/2}$ (min)	1.835	0.8665	3.136	0.5809
$t_{0.95}$ (min)	37.52	27.47	46.31	23.94
R^2 adjusted	0.9992	0.9998	0.9984	0.9998
SD (mg g^{-1})	0.6818	0.5811	1.352	0.7464
Pseudo-first-order				
k_f (min^{-1})	84.25	142.1	113.0	165.3
q_e (mg g^{-1})	0.1974	0.2777	0.1458	0.3166
$t_{1/2}$ (min)	3.512	2.496	4.753	2.189
$t_{0.95}$ (min)	15.18	10.79	20.54	9.462
R^2_{adj}	0.9711	0.9842	0.9663	0.9872
SD (mg g^{-1})	4.189	5.179	6.164	5.394
Pseudo-second-order				
k_s (g mg^{-1} min^{-1})	90.37	149.4	123.5	172.6
q_e (mg g^{-1})	0.003829	0.003771	0.001872	0.004048
$t_{1/2}$ (min)	2.716	1.707	3.945	1.387
$t_{0.95}$ (min)	33.44	24.18	41.90	20.63
R^2_{adj}	0.9973	0.9993	0.9963	0.9993
SD (mg g^{-1})	1.281	1.114	2.034	1.282
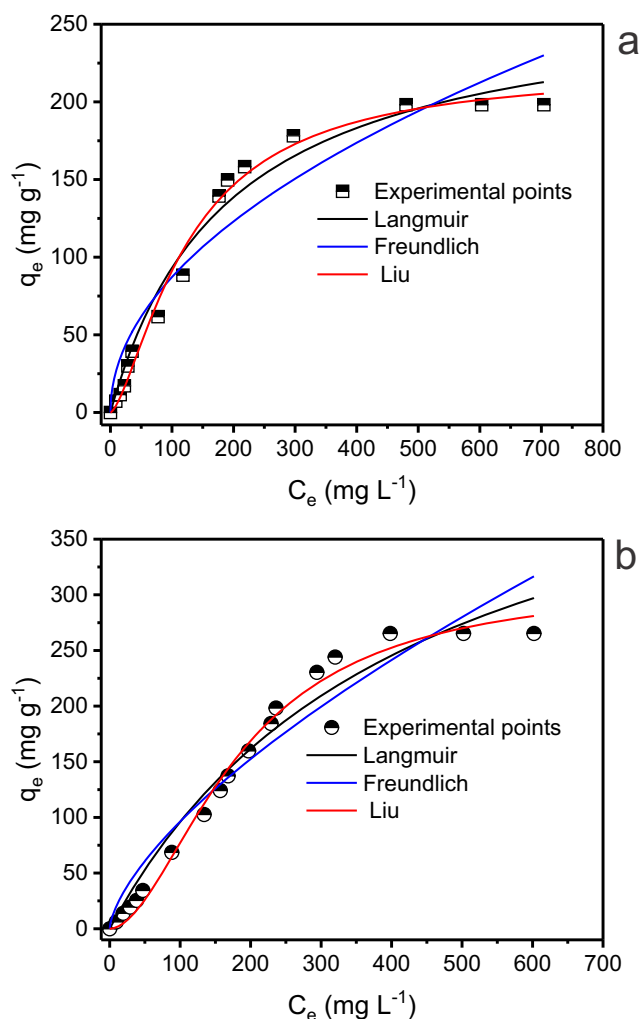
Fig. 8 Equilibrium isotherm curves of (**a**) ASA and (**b**) DFC on *Cpa*-AC. Conditions: pH = 4.0; T = 25 °C; t = 60 min; and mass = 60 mg

Table 2 Isotherm parameters, R^2_{adj}, and SD for ASA and DFC adsorption onto *Cpa*-AC

Nonlinear Models	Pharmaceuticals compounds	
	ASA	DFC
Langmuir		
Q_{max} (mg g^{-1})	270.2	509.8
K_L (L mg^{-1})	0.005261	0.002321
R^2_{adj}	0.9784	0.9702
SD (mg g^{-1})	11.52	17.23
Freundlich		
K_F (mg g^{-1} (mg L^{-1})$^{-1/nF}$)	8.840	4.544
n_F	2.012	1.508
R^2_{adj}	0.9169	0.9373
SD (mg g^{-1})	22.58	24.97
Liu		
Q_{max} (mg g^{-1})	221.7	312.4
K_g (L mg^{-1})	0.007854	0.005457
n	1.477	1.843
R^2_{adj}	0.9899	0.9900
SD (mg g^{-1})	7.871	9.952

leads to fast kinetics. The majority percentage of the mesopore (77.52%) present on *Cpa*-AC favors the fast diffusion of smaller molecules such as ASA and DFC into its network. The estimation of time to attain the equilibrium was based on the $t_{0.95}$ (Umpierres et al. 2018; Kasperiski et al. 2018b) calculated based on the best fitted kinetic model (Avrami fractional-order). The $t_{0.95}$ means the time to arrive at 95% of the saturation, making an interpolation of the modeled kinetic curve. Also, values of $t_{0.5}$ are available in Table 1. This time is useful to estimate the time necessary to achieve 50% of saturation (Umpierres et al. 2018; Kasperiski et al. 2018b). It gives an idea of the initial sorption rate.

Equilibrium experimental studies

The Freundlich, Langmuir, and Liu isotherm models were employed to explore the equilibrium adsorption data (Lima et al. 2012; Kasperiski et al. 2018b). The experimental studies were done employing the best adsorption conditions previously obtained, 60.0 min of contact time, the temperature of 25 °C, a mass of adsorbent of 60.0 mg, and initial pH of pharmaceuticals fixed at 4.0 (see Fig. 8 a and b for ASA and DFC, respectively).

The Liu isotherm presented R^2_{adj} closer to 1.000 and lower SD values (see Table 2), suggesting being the best fitted isotherm model. The SD values were 7.871–9.952 (Liu), 11.52–17.23 (Langmuir), and 22.58–24.97 mg g^{-1} (Freundlich) for ASA and DCF, respectively. Thus, the mathematical model that best describes the equilibrium data of the ASA and DFC was the Liu isotherm model. The maximum sorption capacities (Q_{max}) obtained by the Liu model were 221.7 mg g^{-1} (ASA) and 312.4 mg g^{-1} (DFC).

In order to compare the maximum sorption capacities (Q_{max}) of different adsorbents for acetylsalicylic acid (ASA) and sodium diclofenac (DFC), Table 3 presented a list of different adsorbents that brings this comparison (Bó et al. 2019; Hoppen et al. 2019; Moaca et al. 2019; Jung et al. 2019; Elamin et al. 2019; Gil et al. 2018; Wong et al. 2018a, b; Bhadra et al. 2016; Larous and Meniai 2016; Sathishkumar et al. 2015; Baccar et al. 2012; Saucier et al. 2015; dos Reis et al. 2016a, b; Zhuanga et al. 2020). For ASA, out of ten different adsorbents, including *Cpa*-AC, the proposed adsorbent presented a higher sorption capacity than eight. For DCF for ten different adsorbents (considering *Cpa*-AC), the proposed adsorbent presented the highest sorption capacity. This table is an indication that the *Cpa*-AC could be successfully used in real wastewater treatment.

Table 3 Comparison of maximum sorption capacities (Q_{max}) for adsorption of ASA and DCF

	Q_{max} (mg g^{-1})	Ref
Acetylsalicylic acid (ASA)		
Activated carbon from fruit rinds of *Hymenaea stigonocarpa*	57.1	Bó et al. 2019
Commercial activated carbon	238.7	Bó et al. 2019
Activated carbon of babassu coconut mesocarp	63.2	Hoppen et al. 2019
Composite Fe$_3$O$_4$@C (C - coal)	234	Moaca et al. 2019
Marine macroalgae-derived activated carbon/iron oxide magnetic composites	127	Jung et al. 2019
Functionalized (FMCNT) multiwall carbon nanotubes	58	Elamin et al. 2019
Pristine multiwall carbon nanotubes (PMCNT)	41	Elamin et al. 2019
Commercial activated carbon	33	Gil et al. 2018
Activated carbon from spent tea leaves	178.6	Wong et al. 2018a, b
Lovegrass-activated carbon	221.7	This work
Sodium Diclofenac (DCF)		
Commercial activated carbon	64	Gil et al. 2018
Commercial activated carbon	83	Bhadra et al. 2016
Activated carbon prepared from olive stones	11	Larous and Meniai 2016
Modified phyto-waste *Terminalia catappa* fruit shells	78.5–96.1	Sathishkumar et al. 2015
Olive-waste cake-activated carbon	56.2	Baccar et al. 2012
Microwave-assisted cocoa-activated carbon	63.5	Saucier et al. 2015
Sewage sludge-activated carbon	86.7–157.4	dos Reis et al. 2016a
Composite of polysiloxane and sewage sludge	16.3–41.4	dos Reis et al. 2016b
Covalent organic frameworks (COFs)	70.6	Zhuanga et al. 2020
Lovegrass-activated carbon	312.4	This work

Conclusions

In this work, an efficient and new activated carbon was produced from Annoni grass (*Cpa*) botanically known as *Eragrostis plana* Nees by conventional pyrolysis and ZnCl$_2$ activation. The derived activated carbon called *Cpa*-AC exhibits 71.77% carbon, 2.69% hydrogen, 2.33% nitrogen, and 17.50% oxygen. The *Cpa*-AC material presented the eminent total pore volume (0.6030 g cm^{-3}) and specific surface area (1040 m^2 g^{-1}). FTIR analysis reveals that the chemical groups such as O-H, (C=O) O, N-H, C-O, and aromatic ring are present in the bulk and surface of *Cpa*-AC adsorbent. The *Cpa*-AC adsorbent has 77.52% of mesopores and 22.52% of micropores. The pore size distribution analysis confirms the pores region of mesopores. Boehm titration showed the predominance of acid groups (1.540 mmol g^{-1}) on the surface of *Cpa*-AC adsorbent. The *Cpa*-AC adsorbent presents irregular pores and cavities over the surface. The value of pHPCZ of *Cpa*-AC adsorbent found was 4.96.

The adsorption of ASA and DCF onto *Cpa*-AC adsorbent occurs due to electrostatic interactions and π-π interactions between the *Cpa*-AC and the adsorbate from the solution. Kinetics studies found that the time necessary to reach equilibrium was 45 and 60 min for ASA and DCF, respectively. The isotherm and kinetic adsorption model that best fitted the experimental data were Liu isotherm and Avrami fractional-order kinetic model, respectively. The maximum sorption capacities (Q_{max}) were 221.7 mg g^{-1} (ASA) and 312.4 mg g^{-1} (DCF) using the best adsorption conditions. The results showed that *Cpa*-AC could be used as an alternative and efficiency adsorbent to the existing adsorbent for ASA and DCF removal. Therefore, this work collaborates in research to develop new adsorbent materials employed for the removal of pharmaceutical contaminants from aqueous media.

References

Baccar R, Sarrà M, Bouzid J, Feki M, Blánquez P (2012) Removal of pharmaceutical compounds by activated carbon prepared from the agricultural by-product. Chem Eng J 211-212:310–317

Barbosa FG, Pillar VD, Palmer AR, Melo AS (2013) Predicting the current distribution and potential spread of the exotic grass Eragrostis plana Nees in South America and identifying a bioclimatic niche shift during an invasion. Austral Ecology 38:260–267

Bhadra BN, Seo PW, Jhung SH (2016) Adsorption of diclofenac sodium from water using oxidized activated carbon. Chem Eng J 301:27–34

Bhomick PC, Supong A, Baruah M, Pongener C, Gogoi C, Sinha D (2020) Alizarin red S adsorption onto biomass-based activated carbon: optimization of adsorption process parameters using Taguchi experimental design. Intern J Environ Sci Technol 17:1137–1148

Bó LG, Almeida RM, Cardoso CMM, Zavarize DG, Brum SS, Mendonça ARV (2019) Acetylsalicylic acid biosorption onto fungal-bacterial biofilm supported on activated carbons: an

investigation via batch and fixed-bed experiments. Environ Scie Pollut Res 26:28962–28976

Bolong N, Ismail AF, Salim MR, Matsuura T (2009) A review of the effects of emerging contaminants in wastewater and options for their removal. Desalination 239:229–246

Briton BGH, Yao BK, Richardson Y, Duclaux L, Reinert L, Soneda Y (2020) Optimization by using response surface methodology of the preparation from plantain spike of a micro−/mesoporous activated carbon designed for removal of dyes in aqueous solution. Arab J Sci Eng:1–15. https://doi.org/10.1007/s13369-020-04390-0

Chayid MA, Ahmed MJ (2015) Amoxicillin adsorption on microwave prepared activated carbon from Arundo donax Linn: isotherms, kinetics, and thermodynamics studies. J Environ Chem Eng 3:1592–1601

Chun SY, Chung WJ, Kim SS, Kim JT, Chang SW (2015) Optimization of the TiO_2/Ge composition by the response surface method of photocatalytic degradation under ultraviolet–irradiation and the toxicity reduction of amoxicillin. J Ind Eng Chem 27:291–296

Cunha MR, Lima EC, Cimirro NFGM, Thue PS, Dias SLP, Gelesky MA, Dotto GL, dos Reis GS, Pavan FA (2018) Conversion of Eragrostis plana Nees leaves to activated carbon by microwave-assisted pyrolysis for the removal of organic emerging contaminants from aqueous solutions. Environ Sci Pollut Res 25:23315–23327

Deegan AM, Shaik B, Nolan K, Urell K, Oelgemöller M, Tobin J, Morrissey A (2011) Treatment options for wastewater effluents from pharmaceutical companies. Int J Environ Sci Technol 8:649–666

dos Reis GS, Mahbub MKB, Wilhelm M, Lima EC, Sampaio CH, Saucier C, Dias SLP (2016a) Activated carbon from sewage sludge for removal of sodium diclofenac and nimesulide from aqueous solutions. Korean J Chem Eng 33:3149–3161

dos Reis GS, Sampaio CH, Lima EC, Wilhelm M (2016b) Preparation of novel adsorbents based on combinations of polysiloxanes and sewage sludge to remove pharmaceuticals from aqueous solutions. Colloids Surfaces A 497:304–315

Elamin MR, Abdulkhair BY, Elzupir AO (2019) Insight to aspirin sorption behavior on carbon nanotubes from aqueous solution: thermodynamics, kinetics, the influence of functionalization and solution parameters. Sci Rep 9:12795–12710. https://doi.org/10.1038/s41598-019-49331-6

Elmolla ES, Chaudhuri M (2010) Degradation of amoxicillin, ampicillin, and cloxacillin antibiotics in aqueous solution by the UV/ZnO photocatalytic process. J Hazard Mater 173:445–449

The European Community, Directive 2015, 2015/495/EU of the European Parliament and of the Council of 20 March 2015 establishing a watch list of substances for union-wide monitoring in the field of water policy pursuant to Directive 2008/105/EC.Off, J. Eur. Commun. L78/40

Fatta-Kassinos D, Meric S, Nikolaou A (2011) Pharmaceutical residues in environmental waters and wastewater: current state of knowledge and future research. Anal Bioanal Chem 399:251–275

Filho ACD, Mazzocato AC, Dotto GL, Thue PS, Pavan FA (2017) Eragrostis plana Nees as a novel eco-friendly adsorbent for removal of crystal violet from aqueous solutions. Environ Sci Pollut Res 24:19909–19919

Gil A, Taoufik N, García AM, Korili AS (2018) Comparative removal of emerging contaminants from aqueous solution by adsorption on activated carbon. Environ Technol 40:3017–3030

Ginebreda A, Muñoz I, López de Alda M, Brix R, López-Doval J, Barceló D (2010). Environmental risk assessment of pharmaceuticals in rivers: relationships between hazard indexes and aquatic macroinvertebrate diversity indexes in the Llobregat River (NE Spain) environment International 36: 153–162

Gonzáles-Garcia P (2018) Activated carbon from lignocellulosic precursor: a review of the synthesis methods. Characterization techniques and applications, Renewable and Sustainable Energy Reviews 82: 1393–1414

Homayoonfal M, Mehrnia MR (2014) Amoxicillin separation from pharmaceutical solution by pH-sensitive nanofiltration membranes. Sep Purif Technol 130:74–83

Homem V, Alves A, Santos L (2013) Microwave-assisted Fenton's oxidation of amoxicillin. Chem Eng J 220:35–44

Hoppen MI, Carvalho KQ, Ferreira RC, Passig FH, Pereira IC, Rizzo-Domingues RCP, Lenzi MK, Bottini RCR (2019) Adsorption and desorption of acetylsalicylic acid onto activated carbon of babassu coconut mesocarp. J Environ Chem Eng 7:102862. https://doi.org/10.1016/j.jece.2018.102862

Huerta-Fontela M, Galceran MT, Ventura F (2011) Occurrence and removal of pharmaceuticals and hormones through drinking water treatment. Water Res 45:1432–1442

Jung KW, Choi BH, Song KG, Choi JW (2019) Statistical optimization of preparing marine macroalgae derived activated carbon/iron oxide magnetic composites for sequestering acetylsalicylic acid from aqueous media using response surface methodologies. Chemosphere 215:432–443

Kasperiski FM, Lima EC, dos Reis GS, da Costa JB, Dotto GL, Dias SLP, Cunha MR, Pavan FA, Correa CS (2018a) Preparation of CTAB-functionalized aqai stalk and its efficient application as an adsorbent for the removal of direct blue 15 and direct red 23 dyes from aqueous media. Chem Eng Commun 205:1520–1536

Kasperiski FM, Lima EC, Umpierres CS, dos Reis GS, Thue OS, Lima DR, Dias SLP, Saucier C, da Costa JB (2018b) Production of porous activated carbons from Caesalpinia ferrea seed pod wastes: highly efficient removal of captopril from aqueous solutions. J Clean Prod 197:919–929

Kummerer K (2001) Drugs in the environment: emission of drugs, diagnostic aids, and disinfectants into wastewater by hospitals in relation to other sources – a review. Chemosphere 45:957–969

Larous S, Meniai AH (2016) Adsorption of Diclofenac from aqueous solution using activated carbon prepared from olive stones. Int J Hydrogen Energ 41:10380–10390

Leite AB, Saucier C, Lima EC, dos Reis GS, Umpierres CS, Mello BL, Shirmardi M, Dias SLP, Sampaio CH (2018) Activated carbons from avocado seed: optimization and application for removal several emerging organic compounds. Environ Sci Pollut Res 25:7647–7661

Lima EC, Adebayo MA, Machado FM (2012-5) Chapter 3-kinetic and equilibrium models of adsorption, in Carbon nanomaterials as adsorbents for environmental and biological applications, ed. by C.P. Bergmann, F.M. Machado (Springer, Berlin, 2015), pp. 33–69

Lima EC, Barbosa-Jr F, Krug FJ (2000) The use of tungsten–rhodium permanent chemical modifier for cadmium determination in decomposed samples of biological materials and sediments by electrothermal atomic absorption spectrometry. Anal Chim Acta 409: 267–274

Lima EC, Barbosa-Jr F, Krug FJ, Guaita FJ (1999) Tungsten-rhodium permanent chemical modifier for lead determination in digests of biological materials and sediments by electrothermal atomic absorption spectrometry. J Anal At Spectrom 14:1601–1605

Lima EC, Fenga PG, Romero JR, de Giovani WF (1998a) Electrochemical behavior of $[Ru(4,4'\text{-}Me_2bpy)_2(PPh_3)(H_2O)](ClO_4)_2$ in homogeneous solution and incorporated into carbon paste electrodes. Application to Oxidation of Benzylic Compounds Polyhedron 17:313–318

Lima EC, Krug FJ, Nóbrega JA, Nogueira ARA (1998b) Determination of ytterbium in animal faeces by tungsten coil electrothermal atomic absorption spectrometry. Talanta 47:613–623

Lima DR, Lima EC, Umpierres CS, Thue PS, El-Chaghaby GA, da Silva RS, Pavan FA, Dias SLP, Biron C (2019) Removal of amoxicillin from simulated hospital effluents by adsorption using activated carbons prepared from capsules of cashew of Para. Environ Sci Pollut Res 26:16396–16408

Lima EC, Brasil JL, Santos AHDP (2003) Evaluation of Rh, Ir, Ru, W-Rh, W-Ir, and W-Ru as permanent modifiers for the determination of lead in ashes, coals, sediments, sludges, soils, and freshwaters by electrothermal atomic absorption spectrometry. Anal Chim Acta 484:233–242

Liu W, Wang X, Zhang M (2017) Preparation of highly mesoporous wood-derived activated carbon fiber and the mechanism of its porosity development. Holzforschung 71:363–371

Marques SCR, Marcuzzo JM, Baldan MR, Mestre AS, Carvalho AP (2017) Pharmaceuticals removal by activated carbons: role of morphology on cyclic thermal regeneration. Chem Eng J 321:233–244

Moaca EA, Mihali CV, Macasoi IG, Racoviceanu-Babuta R, Soica C, Dehelean CA, Pacurariu C, Florescu S (2019) Fe3O4@C matrix with tailorable adsorption capacities for paracetamol and acetylsalicylic acid: synthesis, characterization, and kinetic modeling. Molecules 24:1727. https://doi.org/10.3390/molecules2409172

Moussavi G, Alahabadi A, Yagheian K, Eskandari M (2013) Preparation, characterization, and adsorption potential of the NH4Cl-induced activated carbon for the removal of amoxicillin antibiotic. Chem Eng J 217:119–128

Oickle AM, Goertzen SL, Hopper KR, Abdalla YO, Andreas HA (2010) Standardization of the Boehm titration: part II. Method of agitation, the effect of filtering and dilute titrant, Carbon 48: 3313–3322

Pavan FA, Gobbi SA, Moro CC, Costa TMH, Benvenutti EV (2002) The influence of the amount of fluoride catalyst on the morphological properties of the aniline-propyl silica xerogel prepared in basic medium. J Porous Mater 9:307–311

Pavan FA, Lima EC, Dias SLP, Mazzocato AC (2008) Methylene blue biosorption from aqueous solutions by yellow passion fruit waste. J Hazard Mater 150:703–712

Pouretedal HR, Sadegh N (2014) Effective removal of amoxicillin, cephalexin, tetracycline and penicillin G from aqueous solutions using activated carbon nanoparticles prepared from vine wood. J Water Process Eng 1:64–73

Puchana-Rosero MJ, Adebayo MA, Lima EC, Machado FM, Thue PS, Vaghetti JCP, Umpierres CS, Gutterres M (2016) Microwave-assisted activated carbon obtained from the sludge of tannery-treatment effluent plant for removal of leather dyes, Colloid Surf. A 504: 105–115

Sathishkumar P, Arulkumar M, Ashokkumar V, Yusoff ARM, Murugesan K, Palvannan T, Salam Z, Ani FN, Hadibarata T (2015) Modified phyto-waste Terminalia catappa fruit shells: a reusable adsorbent for the removal of micropollutant diclofenac. RSC Adv 5:30950–30962

Saucier C, Adebayo MA, Lima EC, Cataluña R, Thue PS, Prola LDT, Puchana-Rosero MJ, Machado FM, Pavan FA, Dotto GL (2015) Microwave-assisted activated carbon from the cocoa shell as an adsorbent for removal of sodium diclofenac and nimesulide from aqueous effluents. J Hazard Mater 289:18–27

Scheffer-Basso SM, Cecchin K, Favaretto A (2016) Dynamic of dominance, growth, and bromatology of Eragrostis plana Nees in secondary vegetation area. Rev Cienc Agron 47:582–588

Secondes MFN, Naddeo V, Belgiorno V, Ballesteros F Jr (2014) Removal of emerging contaminants by simultaneous application of membrane ultrafiltration, activated carbon adsorption, and ultrasound irradiation. J Hazard Mater 264:342–349

Sophia AC, Lima EC (2018) Removal of emerging contaminants from the environment by adsorption. Ecotoxicol Environ Saf 150:1–17

Sotelo JL, Ovejero G, Rodríguez A, Álvarez S, Galán J, García J (2014) Competitive adsorption studies of caffeine and diclofenac aqueous solutions by activated carbon Chem. Eng J 240: 443–453

Sotelo JL, Rodríguez A, Alvarez S, García J (2012) Removal of caffeine and diclofenac on activated carbon in a fixed-bed column. Chem Eng Res Des 90:967–974

Suriyanon N, Punyapalakul P, Ngamcharussrivichai C (2013) Mechanistic study of diclofenac and carbamazepine adsorption on functionalized silica-based porous materials. Chem Eng J 214:208–218

Taylor D, Senac T (2014) Human pharmaceutical products in the environment – the "problem" in perspective. Chemosphere 115:95–99

Thue PS, Adebayo MA, Lima EC, Sieliechi JM, Machado FM, Dotto GL, Vaghetti JCP, Dias SLP (2016) Preparation, characterization, and application of microwave-assisted activated carbons from wood chips for removal of phenol from aqueous solution. J Mol Liq 223:1067–1080

Tsai WT, Bai YC, Lin YQ, Lai YC, Tsai CH (2020) Porous and adsorption properties of activated carbon prepared from cocoa pod husk by chemical activation. Biomass Convers Bioref 10:35–43

Umpierres CS, Thue PS, dos Reis GS, de Brum IAS, Lima EC, de Alencar WA, Dias SLP, Dotto G (2018) Microwave activated carbons from Tucumã (Astrocaryum aculeatum) waste for efficient removal of 2- nitrophenol from aqueous solutions. Environ Technol 39:1173–1187

Wamba AGN, Ndi SK, Lima EC, Kayem JG, Thue PS, Costa TMH, Quevedo AB, Benvenutti EV, Machado FM (2019) Preparation, characterization of titanate nanosheet–pozzolan nanocomposite and its use as an adsorbent for removal of diclofenac from simulated hospital effluent. J Taiwan Inst Chem Eng 102:321–329

Wang T, Tan S, Liang C (2009) Preparation and characterization of activated carbon from wood via microwave-induced ZnCl2 activation. Carbon 47:1880–1883

Wong S, Lee Y, Ngadi N, Inuwa IM, Mohamed NB (2018a) Synthesis of activated carbon from spent tea leaves for aspirin removal. Chinese J Chem Eng 26:1003–1011

Wong S, Ngadi N, Inuwa IM, Hassan (2018b) Recent advances in applications of activated carbon from biowaste for wastewater treatment: a short review J. Cleaner Prod 175: 361–375

Yacob AR, Azmi A, Mustajab MKAA (2015) Physical and chemical activation effect on activated carbon prepared from local pineapple waste. Appl Mec Mater 699:87–92

Zhuanga S, Chenb R, Liuc Y, Jianlong (2020) Magnetic COFs for the adsorptive removal of diclofenac and sulfamethazine from aqueous solution: adsorption kinetics, isotherms study, and DFT calculation. J Hazard Mater 385:125196. https://doi.org/10.1016/j.jhazmat.2019.121596

Zuccato E, Castiglioni S, Bagnati R, Melis M, Fanelli R (2010) Source, occurrence, and the fate of antibiotics in the Italian aquatic environment. J Hazard Mater 179:1042–1048